http://dx.doi.org/10.5935/0100-4042.20150024 *Quim. Nova,* Vol. 38, No. 4, 518-525, 2015

Artigo

TUNGSTOPHOSPHORIC ACID HETEROGENIZED ONTO NH_4ZSM5 AS AN EFFICIENT AND RECYCLABLE CATALYST FOR THE PHOTOCATALYTIC DEGRADATION OF DYES

Candelaria Leal Marchena[a,c], Silvina Gomez[a,c], Clara Saux[a,c], Liliana B. Pierella[a,c,#] and Luis R. Pizzio[b,c,*]

[a]Centro de Investigación y Tecnología Química, Facultad Regional Córdoba, Universidad Tecnológica Nacional. Maestro López esq. Cruz Roja Argentina, (5016) Córdoba, Argentina

[b]Centro de Investigación y Desarrollo en Ciencias Aplicadas "Dr. J. J. Ronco", Departamento de Química, Facultad de Ciencias Exactas, UNLP-CCT La Plata, (1900) La Plata, Argentina

[c]CONICET (Consejo Nacional de Investigaciones Científicas y Técnicas), Argentina

Recebido em 23/10/2014; aceito em 22/12/2014; publicado na web em 05/03/2015

Materials based on tungstophosphoric acid (TPA) immobilized on NH_4ZSM5 zeolite were prepared by wet impregnation of the zeolite matrix with TPA aqueous solutions. Their concentration was varied in order to obtain TPA contents of 5%, 10%, 20%, and 30% w/w in the solid. The materials were characterized by N_2 adsorption-desorption isotherms, XRD, FT-IR, ^{31}P MAS-NMR, TGA-DSC, DRS-UV-Vis, and the acidic behavior was studied by potentiometric titration with n-butylamine. The BET surface area (S_{BET}) decreased when the TPA content was raised as a result of zeolite pore blocking. The X-ray diffraction patterns of the solids modified with TPA only presented the characteristic peaks of NH_4ZSM5 zeolites, and an additional set of peaks assigned to the presence of $(NH_4)_3PW_{12}O_{40}$. According to the Fourier transform infrared and ^{31}P magic angle spinning-nuclear magnetic resonance spectra, the main species present in the samples was the $[PW_{12}O_{40}]^{3-}$ anion, which was partially transformed into the $[P_2W_{21}O_{71}]^{6-}$ anion during the synthesis and drying steps. The thermal stability of the NH_4ZSM5TPA materials was similar to that of their parent zeolites. Moreover, the samples with the highest TPA content exhibited band gap energy values similar to those reported for TiO_2. The immobilization of TPA on NH_4ZSM5 zeolite allowed the obtention of catalysts with high photocatalytic activity in the degradation of methyl orange dye (MO) in water, at 25 °C. These can be reused at least three times without any significant decrease in degree of degradation.

Keywords: Tungstophosphoric acid; NH_4ZSM5 zeolite; methyl orange; photocatalytic degradation.

INTRODUCTION

The color of wastes is considered the most apparent indicator of waste pollution and it should be reduced before their release into the environment. The presence of small amounts of dyes (below 1 ppm) is clearly visible and considerably influences the water environment.[1] The release of those colored wastewaters into the ecosystem is a dramatic source of esthetic pollution, eutrophication and perturbations in the aquatic life. Wastewaters generated by the textile industries are known to contain considerable amounts of non-fixed dyes, especially of azo dyes, and a huge amount of inorganic salts. It is well known that some azo dyes and degradation products such as aromatic amines are highly carcinogenic.[2]

Recent investigations revealed that reactive dyes could be decolorized by advanced oxidation processes (AOPs). These ambient temperature processes refer to the generation of highly reactive hydroxyl radicals that are aggressive and almost indiscriminately attack all types of inorganic and organic pollutants found in wastewaters. Heterogeneous photocatalysis has appeared as an emerging potential technology for the destruction of organic contaminants in water such as aromatic compounds that present a potential hazard to the environment.[3-5]

Many semiconductor materials have been examined as heterogeneous photocatalysts. However, besides TiO_2, which is claimed as one of the most appropriate semiconductor materials to be employed as a photocatalyst, heteropolyoxometalates (POM) are receiving more attention as photocatalysts. POM were employed as effective homogeneous photocatalysts in the degradation of organic pollutants in water.[6-9]

POM absorb strongly in the near visible and UV region of the light spectrum ($\lambda < 400$ nm). This absorption corresponds to the ligand-to-metal charge-transfer band and it can generate strongly oxidizing excited state POM* (reaction 1). They are able to carry out the oxidation of organic substrates (S) (reaction 2) directly via charge transfer or H-atom abstraction, or indirectly through the intermediacy of solvent-derived radicals.[9] After that, the corresponding reduced POM are usually reoxidized to their original oxidation state by an electron acceptor such as dioxygen (reaction 3).

$$POM + h\nu \rightarrow POM^* \quad (1)$$

$$POM^* + S \rightarrow POM^- + S^+ \quad (2)$$

$$POM^- + O_2 \rightarrow POM + O_2^- \quad (3)$$

S. Anandan *et al.* encapsulated heteropolytungstic acid into titanium-exchanged HY zeolite and obtained a very active photocatalyst towards the photoreduction of methyl orange.[10] R. Ozer and J. Ferry reported the photocatalytic oxidation results of aqueous 1,2-dichlorobenzene by polyoxometalates supported on NaY Zeolite.[11]

Some of the major drawbacks of POM as catalysts are related to their high solubility in water and polar solvents, low surface area and relatively low thermal stability. Supporting POM on solids with high surface area is a useful method for improving catalytic performance in liquid-solid and gas-solid heterogeneous reactions. For instance, Hu *et al.*[12] have used catalysts based on heteropolyacids supported on silica and alumina, with good results, for the preparation of octyl and nonyl phenol, through the alkylation reaction of phenol with 1-octene and nonene, respectively.

Zeolites consist of a three-dimensional network of metal–oxygen tetrahedra (in a few cases also octahedra) that provide the microporous-sized periodic structure, where the active sites are present.

*e-mail: lrpizzio@quimica.unlp.edu.ar
#alternate e-mail: lpierella@scdt.frc.utn.edu.ar

These materials with well-defined pores, channels and/or cavities are well-known for their shape selectivity properties as well as for their catalytic properties in several technological processes and high deactivation/mechanic resistance.[13]

ZSM-5 (MFI type structure: Mirror Framework Inversion) pentasil zeolites with 5.1–5.6Å pore diameter (classified as microporous aluminosilicate systems with orthorhombic symmetry) and well-defined tubular channels offer high surface area, unique nanoscaled porous structure and ion exchange properties for utilization in the design of efficient photocatalytic systems. The arrangement of cages and channels in these crystalline zeolites allow for placement of molecules in a well- defined and unique spatial arrangement, while they can be used as constrained systems for the preparation of semiconductors with controlled particle size and shape.[14]

Zeolites are reported to provide specific photophysical properties such as the control of charge-transfer and electron-transfer processes.[15,16] Zeolite serves as the support where molecules such as heteropolyacids (HPA) can be stabilized by supporting them onto the zeolite surface, and their specific surface area is known to be largely increased.[17]

In this work we aim to investigate the photocatalytic activity of ZSM-5 zeolite impregnated by HPA such as tungstophosphoric acid, by using methyl orange (MO) as a target degraded compound. MO is a good example of azo dyes and alkaline organic pollutants; it is nonbiodegradable; and has been used as a probe for photocatalytic decolorization, and its degradation process has been analyzed in numerous investigations.[18-22] The effects of pH, TPA content over the activity, the repeatability of the photocatalytic activity, and the catalytic activity of the bulk $(NH_4)_3[PW_{12}O_{40}]$ salt were also analyzed. We present the results of the synthesis of ZSM-5 modified by TPA and the characterization by N_2 adsorption-desorption isotherms, XRD, FT-IR, ^{31}P MAS-NMR, TGA-DSC, DRS-UV-Vis; the acidic behavior was studied by potentiometric titration with n-butylamine. Furthermore, the decolorization of MO in the absence and presence of UV-Vis irradiation was investigated for all prepared samples.

EXPERIMENTAL

Catalyst preparation

ZSM-5 material (Si/Al = 17) was obtained by the hydrothermal crystallization method[23] with some modifications made by our group. Aqueous solution of sodium aluminate ($NaAlO_2$, Johnson Matthey Electronics) was introduced into a silica anhydride (Fluka) solution that was previously prepared by partial dissolution of tetrapropylammonium hydroxide (TPAOH, Fluka) in water. The obtained gel reached a pH > 9 and was maintained at 120-160 °C for 12-16 days under self-generated pressure in an autoclave. Afterwards, reaction products were extracted, washed and dried at 110 °C for 12 h. The structure-directing agent (TPAOH) was desorbed in N_2 atmosphere (20 ml min^{-1}) at programmed temperature (10 °C min^{-1}) from 110 to 520 °C and then it was calcined in air at 500 °C for 12 h to obtain Na-ZSM5. The ammonium form of the material (NH_4ZSM5) was from Na-zeolite by ion exchange with NH_4Cl (1 mol L^{-1}) for 40 h at 80 °C.[24]

The tungstophosphoric acid (TPA) solutions were prepared from $H_3PW_{12}O_{40}.23H_2O$ (Fluka p.a.) using distilled water as solvent. The incorporation of TPA ($H_3PW_{12}O_{40}$) into the zeolite matrix was realized by wet impregnation in a rotary evaporator at 80 °C. The amount of TPA to be deposited onto the surface of the zeolite was varied with the purpose of obtaining a TPA concentration of 5%, 10%, 20%, and 30% by weight in the final solid, named NH_4ZSM5TPA05, NH_4ZSM5TPA10, NH_4ZSM5TPA20 and NH_4ZSM5TPA30, respectively. The solids were dried under vacuum at 80 °C. The TPA content on the NH_4ZSM5TPA samples was estimated as the difference between the W amount contained in the tungstophosphoric acid water solution originally used for the wet impregnation and the amount of W remained in the rotary evaporator after removing the dried samples. The amount of W in the water solutions obtained after the ground solids were extracted was determined by atomic absorption spectrometry using a Varian AA Model 240 spectro-photometer. The calibration curve method was used with standards prepared in the laboratory. The analyses were carried out at a wavelength of 254.9 nm, bandwidth 0.3 nm, lamp current 15 mA, phototube amplification 800 V, burner height 4 mm, and acetylene–nitrous oxide flame (11:14). The results obtained reveal that the TPA contents in the samples were 4.9, 9.7, 19.8, and 29.6% (w/w) for NH_4ZSM5TPA05, NH_4ZSM5TPA10, NH_4ZSM5TPA20, and NH_4ZSM5TPA30, respectively.

For comparative purposes, the ammonium salt of tungstophosphoric acid was synthesized following the method reported by Ito *et al.*[25] An aqueous solution of NH_4Cl [0.055 mol L^{-1}] was added dropwise to ca. 30 ml of an ethanol/water (1:1 v/v) solution of $H_3PW_{12}O_{40}$ [0.025 mol/L] with vigorous stirring to form a white colloidal solution containing well-dispersed $(NH_4)_3PW_{12}O_{40}$ precipitates. The resulting solution was aged for 30 min at a temperature of 25 °C. Then it was dried at 55 °C in a vacuum rotary evaporator to obtain the $(NH_4)_3PW_{12}O_{40}$ salt.

Sample characterization

Textural properties

The specific surface area and the mean pore diameter of the solids were determined from the N_2 adsorption-desorption isotherms at the liquid-nitrogen temperature, obtained using Micromeritics PulseChemisorb 2700 equipment. The solids were previously degassed at 100 ºC for 2 h.

Nuclear magnetic resonance spectroscopy

The ^{31}P magic angle spinning-nuclear magnetic resonance (^{31}P MAS-NMR) spectra were recorded with Bruker Avance II equipment, using the CP/MAS ^{1}H-^{31}P technique. A sample holder of 4 mm diameter and 10 mm in height was employed, using 5 μs pulses, a repetition time of 4 s, and working at a frequency of 121.496 MHz for ^{31}P at room temperature. The spin rate was 8 kHz and several hundred pulse responses were collected. Phosphoric acid 85% was employed as external reference.

Fourier transform infrared spectroscopy

The Fourier transform infrared (FT-IR) spectra of the solids were obtained using a JASCO 5300 spectrometer. The spectra in the lattice vibration region were performed using KBr 0.05% wafer technique and they were carried out from 1800 to 400 cm^{-1} in 16 consecutive registers of 4 cm^{-1} resolution each one.

X-Ray diffraction

The X-Ray diffraction (XRD) patterns were recorded with Philips PW-3020 equipment with a built-in recorder, using CuKα radiation, nickel filter, 20 mA and 40 kV in the high voltage source, and scanning angle between 5 and 50° 2θ at a scanning rate of 2° per min.

Thermogravimetric analysis and differential scanning calorimetry

The TGA-DSC measurements of the solids were carried out using a Shimadzu DT 50 thermal analyzer. The thermogravimetric and differential scanning calorimetry analyses were performed under argon or nitrogen, respectively, using 20–30 mg samples and a heating rate of 10 °C/min. The studied temperature range was 20-700 °C.

Diffuse reflectance spectroscopy

The diffuse reflectance spectra (DRS) of the materials were recorded using a UV-visible Lambda 35, Perkin Elmer spectrophotometer, to which a diffuse reflectance chamber Labsphere RSA-PE-20 with an integrating sphere of 50 mm diameter and internal Spectralon coating is attached, in the 200–800 nm wavelength range.

Potentiometric titration

The number of acid sites and their acid strength were estimated by means of potentiometric titration. A known mass of solid was suspended in acetonitrile and stirred for 3 h. Then, the suspension was titrated with 0.05N n-butylamine in acetonitrile using Metrohm 794 Basic Titrino apparatus with a double junction electrode. The initial electrode potential (E_i) indicates the maximum acid strength of the sites and the value of meq amine/g solid where the plateau is reached indicates the total number of acid sites. The acid strength of these sites may be classified according to the following scale: $E_i > 100$ mV (very strong sites), $0 < E_i < 100$ mV (strong sites), $-100 < E_i < 0$ (weak sites) and $E_i < -100$ mV (very weak sites).[26]

Photocatalytic activity evaluation

The catalytic activity of the materials was evaluated in the photodegradation of methyl orange (Fluka p.a.) in water, at 25 °C. Photocatalytic activity of the materials was carried out in a borosilicate glass reactor. UV-Vis irradiation was provided by a high-pressure mercury lamp Philips HPL-N 125W (with a maximum emission at about 365 nm) placed inside a Pyrex glass jacket, thermostated by water circulation, in order to check any evaporation losses of reaction solution due to the heating effect of the light source.

A measured amount of the photocatalyst was suspended in 400 ml of 2.62 mg/l methyl orange (MO) solution in a Pyrex glass reactor with an inlet for the circulation of air. The solution was stirred on a magnetic stirrer and exposed to irradiation for 4 h. Previously, the MO solution containing a predetermined amount of catalyst was magnetically stirred in the absence of light for 30 min to ensure that the adsorption-desorption equilibrium of MO on the surface of the materials was attained. After the irradiation, the suspension was filtered using 0.45 μm cellulose nitrate filters. Progress of the reaction was measured spectrophotometrically using a Jasco 7800 double-beam UV-Vis spectrophotometer. The concentration change was calculated from the linear calibration plot of MO at a wavelength of 464 nm.

In order to evaluate the possibility of TPA leaching during the photocatalytic degradation of MO, at the end of each experiment, the catalyst was separated by centrifugation, and W was determined in the liquid phase by atomic absorption spectrometry as was explained before.

RESULTS AND DISCUSSION

Physicochemical characterization

In Table 1 the BET surface area (S_{BET}) of the synthesized materials together with NH_4ZSM5 and TPA samples, determined from N_2 adsorption-desorption isotherms (data not shown) using the Brunauer-Emmett-Teller (BET) method, are shown.

The N_2 adsorption-desorption isotherms of the NH_4ZSM5TPA05, NH_4ZSM5TPA10, NH_4ZSM5TPA20, and NH_4ZSM5TPA30 samples exhibit similar characteristics to that of NH_4ZSM5 zeolite. They can be classified as Type I isotherms according to IUPAC, characteristic of microporous solids having relatively small external surfaces. The S_{BET} decreases with the increment of TPA content in the sample.

Table 1. BET surface area, crystallite size and optical band gap of TPA, NH_4ZSM5, and TPA-zeolite samples

Samples	S_{BET} (m^2 g^{-1})	Dc [a] (nm)	E_g (eV)
NH_4ZSM5	355	0.4	5.70
NH_4ZSM5TPA05	337	0.6	3.25
NH_4ZSM5TPA10	335	0.6	3.20
NH_4ZSM5TPA20	322	0.6	3.18
NH_4ZSM5TPA30	323	0.6	3.18
TPA	2	5.0	2.8

[a]Dc values of TPA and NH_4ZSM5 samples were calculated using the (2, 2, 2) and (1, 0, 1) crystal plane, respectively.

Taking into account that $[PW_{12}O_{40}]^{3-}$ anions have a diameter of 1.2 nm,[27] and the pore entrance of NH_4ZSM5 zeolite is 0.56 nm,[28] the progressive decrease of S_{BET} could be due to the clogging of NH_4ZSM5 zeolite pores.

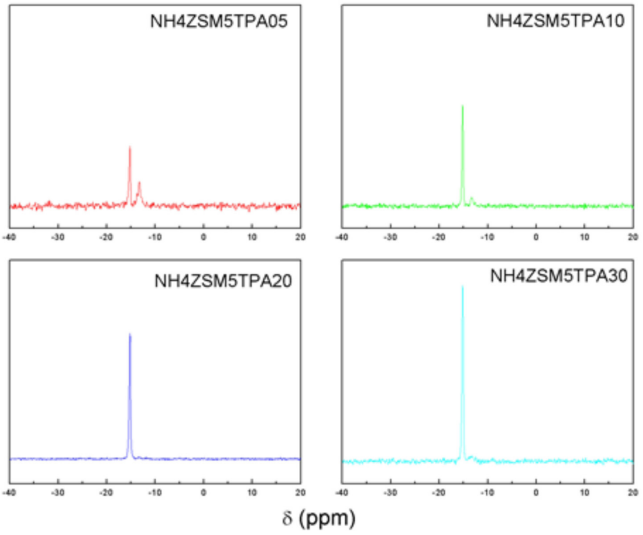

Figure 1. *^{31}P MAS-NMR spectra of NH4ZSM5TPA05, NH4ZSM5TPA10, NH4ZSM5TPA20, and NH4ZSM5TPA30 samples*

The ^{31}P MAS-NMR spectra of NH_4ZSM5TPA05, NH_4ZSM5TPA10, NH_4ZSM5TPA20, and NH_4ZSM5TPA30 samples (Figure 1) show two lines of resonance at -15.2 and -13.4 ppm. These lines can be assigned to the presence of the $[PW_{12}O_{40}]^{3-}$ anion and to the dimeric species $[P_2W_{21}O_{71}]^{6-}$, respectively.[29] The signal corresponding to the $[PW_{12}O_{40}]^{3-}$ anion is, in all cases, the most intense. On the other hand, the intensity of the signal belonging to the dimer $[P_2W_{21}O_{71}]^{6-}$ decreases and practically disappears (NH_4ZSM5TPA20 and NH_4ZSM5TPA30 samples) when the TPA content increases.

We found that the proportion of the Keggin anion $[PW_{12}O_{40}]^{3-}$ in the NH_4ZSM5TPA samples was higher than in those synthesized by using NH_4Y as support.[30] This can be attributed to the higher acidity of NH_4ZSM5 compared to NH_4Y, which reduces the transformation of $[PW_{12}O_{40}]^{3-}$ into $[P_2W_{21}O_{71}]^{6-}$. This transformation is due to the limited stability range of the $[PW_{12}O_{40}]^{3-}$ anion in solution, which can be increased by adding an organic solvent such as ethanol.[31,32]

The FT-IR spectrum of NH_4ZSM5 (Figure 2) shows bands at 1228, 1101, 800, 549, and 453 cm^{-1} due to different vibrations of tetrahedral atoms and the zeolite network. The first two are assigned to asymmetrical stretching vibrations of tetrahedral Si-Al, and the third signal is due to the symmetrical stretching vibration of Si-O. The vibrational band at 549 cm^{-1} confirms the presence of five-member

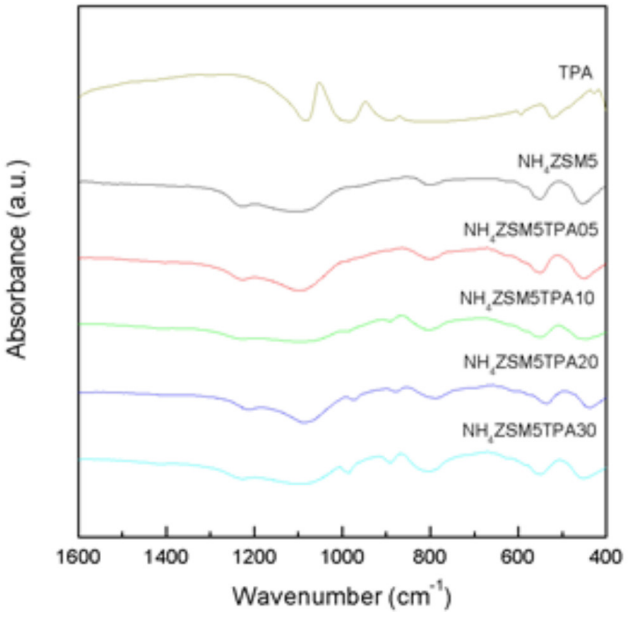

Figure 2. *FT-IR spectra of TPA, $(NH_4)_3PW_{12}O_{40}$, NH_4ZSM5, NH_4ZSM5TPA05, NH_4ZSM5TPA10, NH_4ZSM5TPA20, and NH_4ZSM5TPA30 samples*

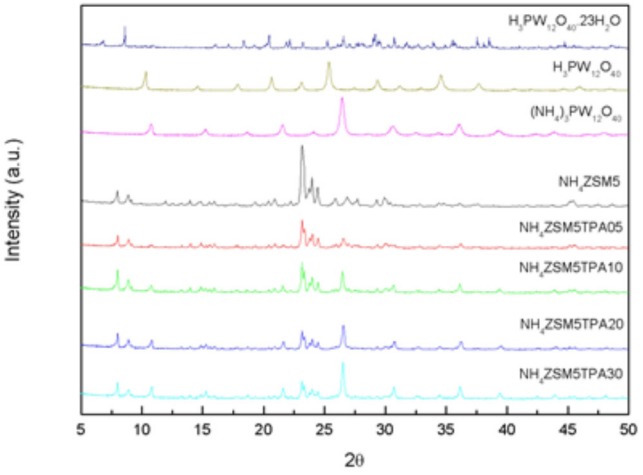

Figure 3. *XRD patterns of $H_3PW_{12}O_{40}\cdot 23H_2O$ (JCPDS 50-0655), $H_3PW_{12}O_{40}$ (JCPDS 50-0657), $(NH_4)_3[PW_{12}O_{40}]$ (JCPDS 50-0305), NH_4ZSM5 (JCPDS 44-0002), and the samples NH_4ZSM5TPA05, NH_4ZSM5TPA10, NH_4ZSM5TPA20 and NH_4ZSM5TPA30*

rings of the pentasil structure. This band is characteristic of the absorption of silicon-oxygen bonds in double rings of 5 members, while the band at 440 cm^{-1} is assigned to the internal T-O_4 (T: Si or Al) tetrahedral bending bonds.[28]

The FT-IR spectrum of TPA (Figure 2) shows bands at 1081, 982, 888, 793, 595, and 524 cm^{-1}, which are in accordance with those reported in the literature for the $H_3PW_{12}O_{40}$ acid.[33] The first five bands are assigned to the stretching vibrations P-O_a, W-O_d, W-O_b-W, W-O_c-W, and to the bending vibration O_a-P-O_a, respectively. The subscripts indicate oxygen bridging W and the P heteroatom (a), corner-sharing (b) and edge-sharing (c) oxygen belonging to WO_6 octahedra, and terminal oxygen (d). The spectrum of the $(NH_4)_3PW_{12}O_{40}$ salt also displays a band at 1415 cm^{-1} assigned to the N-H stretch.

The main FT-IR bands of the dimer $[P_2W_{21}O_{71}]^{6-}$ assigned to the stretching vibrations P-O, W-O, W-O-W appear at wavenumber values similar to those characteristic of the $[PW_{12}O_{40}]^{3-}$ anion,[34] making it difficult to establish its presence on the basis of these spectra only because unfortunately, these signals are below the strong signals of zeolite.

In the spectra of the NH_4ZSM5TPA05, NH_4ZSM5TPA10, NH_4ZSM5TPA20 and NH_4ZSM5TPA30 samples, overlying the characteristic bands of the zeolite appear those assigned to the W-O_d, W-O_b-W, and W-O_c-W stretching vibrations of $[PW_{12}O_{40}]^{3-}$. Their relative intensity increases with the increment of TPA in the materials. The W-O_c-W vibration produces the broadening of the zeolite band at 800 cm^{-1} assigned to the Si-O stretching vibration.[35]

According to ^{31}P MAS-NMR and FT-IR results, the main species present in the samples is the $[PW_{12}O_{40}]^{3-}$ anion, which was partially transformed into the $[P_2W_{21}O_{71}]^{6-}$ anion during the synthesis and drying steps. At pH 1.5–2, it is reversibly and quickly transformed into the lacunar species $[PW_{11}O_{39}]^{7-}$. Pope[32] has proposed that the following transformation scheme: $[PW_{12}O_{40}]^{3-} \Leftrightarrow [P_2W_{21}O_{71}]^{6-} \Leftrightarrow [PW_{11}O_{39}]^{7-}$ takes place when the pH is increased. This may be considered as a valid path followed by the TPA species during the synthesis of the samples.

The XRD patterns of the NH_4ZSM5TPA05, NH_4ZSM5TPA10, NH_4ZSM5TPA20, and NH_4ZSM5TPA30 samples (Figure 3) show the characteristic peaks of NH_4ZSM5 zeolite. However, their intensity decreases in parallel with the increment of TPA content. The XRD patterns also present an additional set of peaks, which are different from those characteristic of the tungstophosphoric acid ($H_3PW_{12}O_{40}$), its more common hydrates ($H_3PW_{12}O_{40}\cdot 23H_2O$ and $H_3PW_{12}O_{40}\cdot 6H_2O$), or other crystalline phases resulting from their transformation.[36] These peaks are similar to those characteristic of the cubic structure of $(NH_4)_3PW_{12}O_{40}$, whose formation takes place as a result of the interaction between $[PW_{12}O_{40}]^{3-}$ anions and $[NH_4]^+$ cations present in the zeolite matrix.

We estimated the crystallite size (D_C) of the NH_4ZSM5TPA05 samples by XRD using the Scherrer equation (Table 1). It seems to be independent of the TPA content in the prepared materials and it is similar to that of parent zeolite.

The interaction between $H_3PW_{12}O_{40}$ and supports such as SiO_2, TiO_2, or ZrO_2 can be assumed to be of the electrostatic type due to the transfer of protons to M-OH according to:[37]

$$\text{M-OH} + H_3PW_{12}O_{40} \rightarrow [\text{M-OH}_2^+]\,[H_2PW_{12}O_{40}^-]$$

It has been reported that proton transfer from TPA to the amine group, resulting in an electrostatic bond between $-NH_3^+$ and $[H_{3-x}PW_{12}O_{40}]^{x-}$ (where $1 < x \leq 3$), is responsible for the efficient immobilization of the heteropolyanion.[38,39]

In the NH_4ZSM5TPA samples, the interaction between $H_3PW_{12}O_{40}$ and ZSM5 zeolite can be described as the electrostatic type due to the interaction of $[H_{3-x}PW_{12}O_{40}]^{x-}$ (where $1< x \leq 3$) anions an the $[NH_4]^+$ cations present in the zeolite matrix.

The DSC diagram of zeolite NH_4ZSM5 (Figure 4a) exhibits an endothermic peak at 45 °C with a shoulder peak at 228 °C, and a second one at 377 °C. They are associated with the elimination of physisorbed water, NH_3 and zeolite structural changes, respectively.[40] From the TGA diagram, we estimated the weight loss associated with the release of physisorbed water and ammonia as 6% of the initial mass, which is in agreement with the results reported by Decolatti *et al.*[41] The weight loss ascribed to structural changes (dehydroxylation) is, in this case, less than 1%.

On the other hand, the DSC diagram of the NH_4ZSM5TPA05, NH_4ZSM5TPA10, NH_4ZSM5TPA20, and NH_4ZSM5TPA30 samples (Figure 4b) presents the endothermic peaks and the shoulder assigned to the elimination of physisorbed water and ammonia, which are in the same temperature range indicated above for the NH_4ZSM5 zeolite

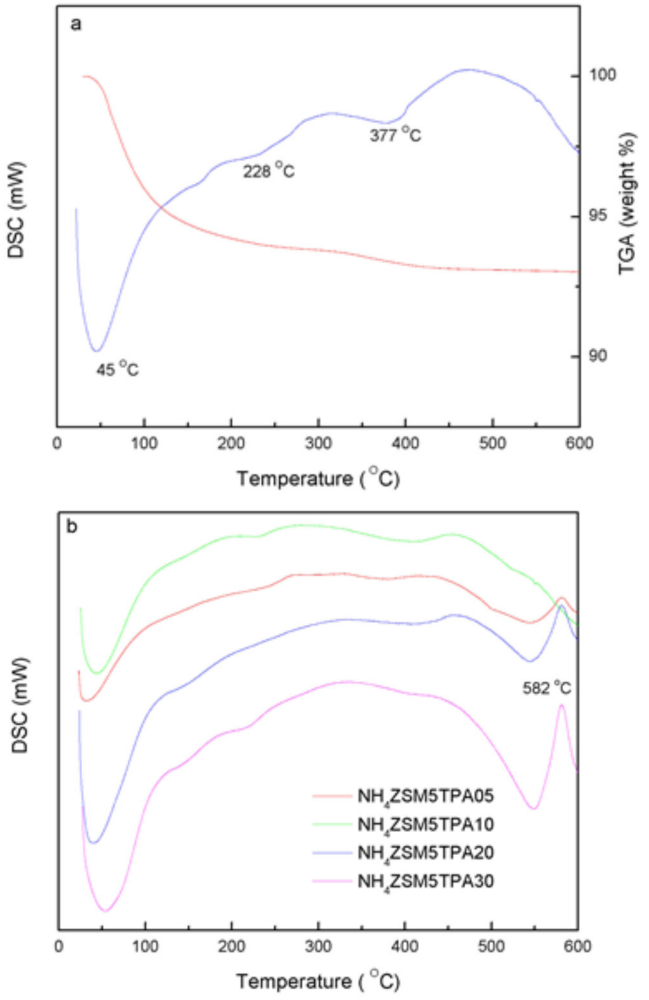

Figure 4. *Thermal analysis diagrams of NH4ZSM5 zeolite (a) and NH_4ZSM5TPA05, NH_4ZSM5TPA10, NH_4ZSM5TPA20, and NH_4ZSM5TPA30 samples (b)*

matrix. However, the peak assigned to structural changes appears displaced to temperatures in the range 400–420 °C in samples with TPA content higher than 5%.

In addition to the above-mentioned peaks, the diagrams of NH_4ZSM5TPA10, NH_4ZSM5TPA20, and NH_4ZSM5TPA30 samples show an exothermic peak with maximum at 582 °C assigned to the decomposition of the Keggin anion $[PW_{12}O_{40}]^{3-}$, whose intensity decreases in parallel with the decrease of TPA content in the samples.

The DSC diagram of $H_3PW_{12}O_{40}.23H_2O$ (see supplementary material) shows that the Keggin anion decomposed at 595 ºC into the constituent oxides or, according to Mioc *et al.*,[36] transformed into a new monophosphate bronze-type compound PW_8O_{26} without appreciable weight loss.

On the other hand, due to the low amount of the dimer present in the solids, the exothermic peak assigned to the $[P_2W_{21}O_{71}]^{6-}$ anion was not detected in this set of samples.[30]

The charge-transfer absorption spectrum of TPA obtained by UV-Vis-DRS present a band at 212 nm and another broad band that extends from 250 to 450 nm[42,43] assigned to the charge transfer from bridging or terminal O 2p to W 5d (W-O-W and W-O_d, respectively). The same characteristics bands are present in the DRS spectrum of the ammonium salt $(NH_4)_3[PW_{12}O_{40}]$ (Figure 5).

The UV-Vis-DRS spectra of the NH_4ZSM5TPA05, NH_4ZSM5TPA10, NH_4ZSM5TPA20, and NH_4ZSM5TPA30 samples, together with that of NH_4ZSM5 zeolite, are shown in Figure 5. The UV-Vis-DRS spectrum of zeolite presents weak absorption between

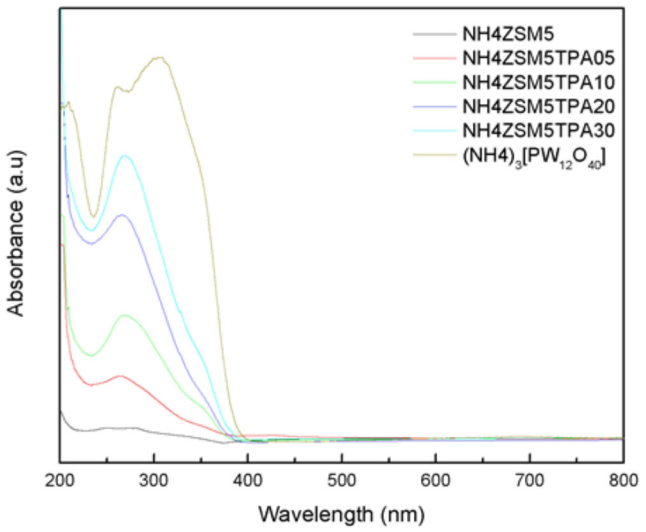

Figure 5. *UV-Vis-DRS spectra of the samples NH_4ZSM5, NH_4ZSM5TPA05, NH_4ZSM5TPA10, NH_4ZSM5TPA20, NH_4ZSM5TPA30 and $(NH_4)_3[PW_{12}O_{40}]$*

200 and 220 nm that arose from the Al-O charge-transfer transition of four–coordinated framework aluminum.[44]

DRS spectra of the NH_4ZSM5TPA05, NH_4ZSM5TPA10, NH_4ZSM5TPA20 and NH_4ZSM5TPA30 samples show that the addition of TPA leads to an increase in the intensity of the band placed at 200 nm and the appearance of a new one at 267 nm, which agrees with the values reported by Fox *et al.*[45] for ammonium salts of the Keggin anion. As a result of the increasing TPA content in the samples, there is a small shift of the absorption threshold onset to the visible region.

The band gap energy values (E_g), estimated from UV-Vis-DRS spectra using Kubelka-Munk remission function,[46] are listed in Table 1. These values are similar to those reported in the literature for TiO_2 samples.[47] The E_g value of NH_4ZSM5 zeolite without TPA is in agreement with those reported in the literature.[48]

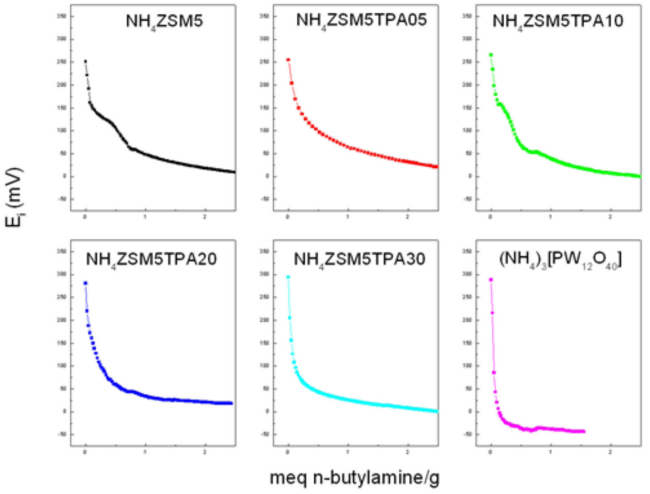

Figure 6. *Potentiometric titration curves of the NH_4ZSM5, NH_4ZSM5TPA05, NH_4ZSM5TPA10, NH_4ZSM5TPA20, and NH_4ZSM5TPA30, and $(NH_4)_3[PW_{12}O_{40}]$*

The titration curves obtained for the NH_4ZSM5TPA05, NH_4ZSM5TPA10, NH_4ZSM5TPA20, and NH_4ZSM5TPA30 samples are shown in Figure 6. The materials present very strong and strong acid sites, with E_i values in the range 254–294 mV. The E_i value increases with the increment of the TPA content according to the following order: NH_4ZSM5 (E_i = 251 mV) < NH_4ZSM5TPA05 (E_i = 254

mV) < NH_4ZSM5TPA10 (E_i = 266 mV) < NH_4ZSM5TPA20 (E_i = 282 mV) < NH_4ZSM5TPA30 (E_i = 294 mV). Additionally, the E_i values of the samples with higher TPA content are close to that of the $(NH_4)_3PW_{12}O_{40}$ salt (E_i= 288 mV), which is significantly lower than the value reported for $H_3PW_{12}O_{40}.21H_2O$ (E_i= 538 mV).[26] On the other hand, the number of acid sites determined by this technique is practically independent of the TPA content and it is similar to that of zeolite. So, the potentiometric titulation reveals that the acid strength of the TPAXX-NH4ZSM5 samples are close to that of the $(NH_4)_3PW_{12}O_{40}$ salt (E_i= 288 mV), which is significantly lower than the value reported for $H_3PW_{12}O_{40}.21H_2O$ (E_i= 538 mV). These results are in agreement with the presence of $(NH_4)_3PW_{12}O_{40}$ whose formation takes place due to the interaction between $[PW_{12}O_{40}]^{3-}$ anions and $[NH_4]^+$ cations present in the zeolite matrix. Additionally, the number of acid sites is practically independent of the TPA content and it is similar to that of zeolite. As a result, the point of zero charge of the samples remains almost constant (PZC in the range 5.3-5.0) in spite of the increment of TPA content from 5 to 30 % (w/w).

Evaluation of photocatalytic activity

Methyl orange (MO), used as a model contaminant, is an azo dye that exhibits acid-base equilibrium in solution with pK_a =3.5. Under neutral conditions, MO exists as negative charged form[49] with orange color (λ_{max} = 464 nm, ε = 24600).[50] The band at 464 nm that is associated with the azo bond (-N=N-) was used to monitor the effect of photocatalysis on the degradation of MO under neutral conditions.

During the photocatalytic oxidation of MO, the oxidative species formed decompose the dye via a pathway from intermediates (see supplementary material) to the final carbon dioxide and some inorganic products (SO_4^{2-}, NO_3^- and NH_4^+).[19] The formation of intermediates occurs through two primary processes: demethylation and hydroxylation.[51] The addition of a hydroxyl radical to the carbon atom linking with the azo bond is the first target for the hydroxyl radical reaction.[52] As a result of this attack, the C–N cleavage occurs,[19] the chromophore group (R_1–N = N–R_2) is destroyed, and the discoloring is observed.

Before the photocatalytic degradation experiments, methyl orange adsorption (in the dark) on the NH_4ZSM5TPA samples was measured under the same experimental conditions. The percentage of MO adsorbed increased during the first 15 min and then remained constant and lower than 10%. The initial and the final pH values of the solutions were in the range 7.7–5.0. Under these experimental conditions MO was present in its negative form, and the surface of the catalysts (point of zero charge in the range 5.0–5.3) was mostly negatively charged. Therefore, the adsorption of MO on the catalyst surface took place at a low degree (lower than 10%). No detectable MO degradation took place after 240 min of irradiation but without catalyst.

Figure 7 shows the variation of MO concentration (C_{MO}) as a function of time using the NH_4ZSM5, NH_4ZSM5TPA05, NH_4ZSM5TPA10, NH_4ZSM5TPA20, and NH_4ZSM5TPA30 samples as catalyst. The diminution of the MO concentration is only 10% for the NH_4ZSM5 sample at 240 min under reaction. However, for the TPA-modified samples, the MO degradation at the same time is significantly higher, and it increases in parallel with the increment of TPA in the following order NH_4ZSM5TPA05 (24%) < NH_4ZSM5TPA10 (50%) < NH_4ZSM5TPA20 (71%) < NH_4ZSM5TPA30 (81%). We can conclude that the MO degradation rates increase when the TPA content is raised, though the increase is lower when the TPA amount changes from 20% to 30%.

The increment of the catalytic activity when the TPA content increases is principally due to the direct participation of TPA in the degradation of the organic substrate (reactions 1–3) and/or in the production of the •OH reactive species (reaction 4) that participates in the degradation of the organic substrate (reaction 5).[53]

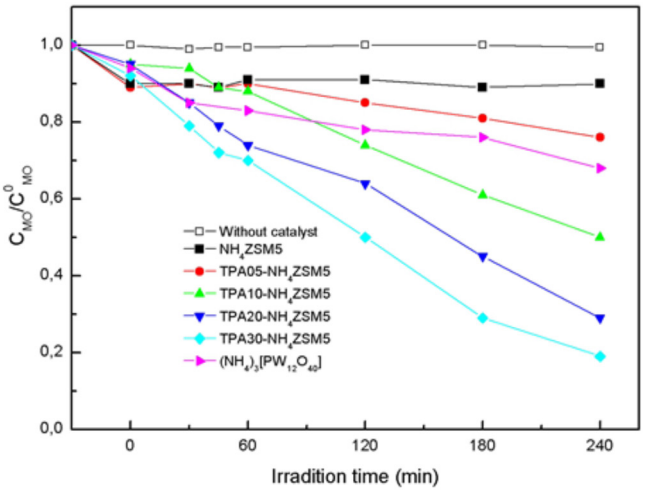

Figure 7. *Photocatalytic degradation of MO as a function of the irradiation time using NH_4ZSM5, NH_4ZSM5TPA05, NH_4ZSM5TPA10, NH_4ZSM5TPA20, NH_4ZSM5TPA30, and $(NH_4)_3[PW_{12}O_{40}]$ as catalyst*

$$POM^* + H_2O \rightarrow POM^- + {}^\bullet OH + H^+ \quad (4)$$

$$^\bullet OH + S \rightarrow \text{oxidation products} \quad (5)$$

For comparison purposes, we measured the catalytic activity of the bulk $(NH_4)_3PW_{12}O_{40}$ salt under the same experimental conditions. In this test, the amount of $(NH_4)_3PW_{12}O_{40}$ was fixed in order to obtain a TPA amount similar to that contained in the NH_4ZSM5TPA30 sample. MO concentration decreased by 32% at 240 min under reaction and it was lower than those obtained using the NH_4ZSM5TPA30 sample. We also measured the catalytic activity of TPA supported (30% w/w in the final solid) on γ-Al_2O_3 (surface area, 280 m^2/g; mean pore diameter 3.4 nm).[32] After 240 min under reaction the MO concentration decreased only 25 %. This could be attributed to the fact that only the $[P_2W_{21}O_{71}]^{6-}$ anion was present in this TPA supported on γ-Al_2O_3.[32] This is in agreement with the fact that at similar TPA content, the sample with lower amount of $[P_2W_{21}O_{71}]^{6-}$ anion showed the higher catalytic activity.[30]

Taking into account the result published by Mizrahi *et al.,*[54] the rather poor catalytic behavior of the $(NH_4)_3PW_{12}O_{40}$ salt could be mainly due to the lower specific surface area of ammonium salt (125 $m^2\ g^{-1}$) in comparison to NH_4ZSM5TPA30 sample (323 $m^2\ g^{-1}$). However, the $(NH_4)_3PW_{12}O_{40}$ salt showed a higher surface area than TPA, due to the smaller sizes of the primary particles (composed by certain number of $[PW_{12}O_{40}]^{3-}$ and NH_4^+ cations) and their three-dimensional arrangement.[32] Additionally, we can suggest that the shape and the size of the $(NH_4)_3[PW_{12}O_{40}]$ crystals should be considered in order to explain the catalytic behaviour of the samples.

On the other hand, we consider that NH4ZSM5 zeolite mainly acts as a suitable support to disperse and fix the TPA. However, we are not able to rule out that the specific photophysical properties ascribed to Y-zeolite such as the control of charge-transfer and electron-transfer processes[15,16] could take place in our samples and enhance the catalytic activy in a certain degree.

The catalyst with the best performance in MO degradation (NH_4ZSM5TPA30) was chosen for further studies.

In order to study TPA leaching, we followed the percentage of MO degraded (C_{DEG}) using NH_4ZSM5TPA30 as catalyst during 60 min. After that, the catalyst was removed by filtration and the solution was irradiated another 180 min. The C_{MO}/C°_{MO} values obtained during the first 60 min of irradiation were similar to those shown in

Figure 7, and the C_{DEG} value equal to 38% was reached at 60 min. However, the percentage of MO degraded remained constant during the irradiation for 180 min after the catalyst removal. According to these results we can rule out that significant TPA solubilization takes place during the reaction.

The effect of catalyst concentration (C_{CAT}) on the degradation rate was studied by varying catalyst concentration from 0.25 to 1.00 g L^{-1} keeping MO concentration constant. It was found that the amount of MO degraded after 240 min (C_{DEG}) increased significantly from 33% to 81% when C_{cat} was raised from 0.25 to 0.50 g L^{-1}. C_{DEG} slightly increased when C_{CAT} was equal to 0.75 g L^{-1} (90%) and it decreased (70%) for higher catalyst concentrations (C_{CAT} = 1.0 g L^{-1}). At C_{CAT} values higher than 0.50 g L^{-1},[55,56] the solution became cloudy, light penetration was reduced and as a result the C_{DEG}/C_{CAT} ratio decreased. Additionally, the C_{CAT} increment may result in the agglomeration of catalyst particles, hence part of the catalyst surface became unavailable for photon absorption and the degradation rate subsequently decreased.

The solution pH is an important variable in aqueous phase mediated photocatalytic reactions because it influences the catalyst surface charge, the adsorption of the substrate, and other physicochemical properties of the system[57]

In order to study the effect of pH on the photocatalytic degradation of methyl orange by NH_4ZSM5TPA30, the experiments were performed at acidic (pH=2.5) and alkaline (pH=9.7) pH values of the MO solution, keeping all other experimental conditions constant. The amount of MO degraded slightly increased at pH= 2.5 (from 81% to 91%) at the same irradiation time (240 min) and it dramatically decreased (from 81% to 32%) at pH=9.7. A similar influence of the pH on the photodegradation of methyl orange was reported[18,21,22] in other reaction systems.

The higher MO amount degraded at acidic pH is due to the increment of the MO adsorbed on the catalyst surface (C_{MOADS}). The C_{MOADS} values increased from 3.2 10^{-6} mol g^{-1} to 8.2 10^{-6} mol g^{-1} when the pH decreased from 5.0 to 2.5. On the other hand, C_{MOADS} decreased from 3.2 10^{-6} mol g^{-1} to 1.2 10^{-6} mol g^{-1} when the pH increased from 5.0 to 9.7.

These results are in agreement with the fact that at pH values lower or higher than pH_{zpc}, the catalyst surface will be positively or negatively charged, and as a result the absorption of negatively charged MO will be favored or impeded, respectively.

The use of TPA immobilized on NH_4ZSM5 zeolite allows an easy separation and recovery of the catalyst for its immediate reutilization. After each reaction, it was recovered by filtration, washed with distilled water and dried at ambient temperature. The catalyst was reused three times. The percentage of MO degraded (C_{DEG}) during the first and the second reuses (65% and 40%, respectively) was significantly lower than the value obtained using the fresh catalyst (90%). The C_{DEG} value reached after the third reuse was practically the same (39%). Taking into account that significant TPA solubilization did not take place during the reaction, the activity loss of the catalyst could be due to the adsorption of degradation products on the catalyst surface.[58] The elimination of degradation products can be achieved by adequate thermal treatment, but this treatment could also induce the sintering of catalyst particles and structural changes resulting in the decrease of photocatalytic activity.

In order to study this possibility, after the third reuse the catalyst was separated by filtration, treated at 400 ºC for 2 h and reused again. Although the C_{DEG} value using the catalyst treated in this way increased (81%), the activity was not completely restored. The XRD pattern and FT-IR spectrum of NH_4ZSM5TPA30 calcined at 400 ºC present similar features to those of the fresh one. Only a small decrease in the BET surface area (S_{BET} = 305 m^2 g^{-1}) was detected and it could be the reason for the slightly smaller photocatalytic activity of the calcined sample.

CONCLUSIONS

Tungstophosphoric acid/NH4ZSM5 zeolite materials were prepared by wet impregnation. According to FT-IR and ^{31}P MAS-NMR results the main species present in the samples is the $[PW12O40]^{3-}$ anion. A small but noticeable transformation into $[P2W21O71]^{6-}$ anion during the synthesis and drying steps took place for the NH4ZSM5TPA05 and NH4ZSM5TPA10 samples.

The S_{BET} of the samples decreased with the increment of the TPA content due to zeolite pore blocking by [PW12O40]3- and [P2W21O71]6- species.

The thermal stability of the NH_4ZSM5TPA samples is similar to that of NH_4ZSM5 zeolite. On the other hand, the decomposition of the anions $[PW12O40]^{3-}$ and $[P_2W_{21}O_{71}]^{6-}$ takes place at temperatures similar to those reported for the bulk compounds.

The addition of TPA generates a red shift of the absorption threshold onset, which is more significant for the samples with the higher TPA content and whose band gap energy values are similar to those reported for TiO2.

The materials obtained by immobilization of TPA onto the zeolite matrix present suitable textural and physicochemical properties to be used as catalysts in the photocatalytic treatment of wastewater that contains azo dyes. The solid containing 30% TPA showed higher photocatalytic activity. On the other hand, the catalyst separated by filtration and treated at 400 ºC for 2 h can be reused without an important decrease in the degradation degree.

ACKNOWLEDGEMENTS

The authors thank Dr. D. Lick, G. Valle and L. Osiglio for their experimental contribution and to CONICET and UNLP for the financial support.

REFERENCES

1. Grzechulska, J.; Morawski, A. W.; *Appl. Catal., B* **2002**, *36*, 45.
2. Brown, M. A.; DeVito, S. C.; *Crit. Rev. Environ. Sci. Technol.* **1993**, *23*, 249.
3. Lachheb, H.; Puzenat, E.; Houas, A.; Ksibi, M.; Elaloui, E.; Guillard, C.; Herrmann, J. M.; *Appl. Catal., B* **2002**, *39*, 75.
4. Nikazar, M.; Gholivand, K.; Mahanpoor, K.; *Desalination* **2008**, *219*, 293.
5. Huang, M.; Xu, C.; Wu, Z.; Huang, Y.; Lin, J.; Wu, J.; *Dyes Pigm.* **2008**, *77*, 327.
6. Mylonas, A.; Hiskia, A.; Papaconstantinou, E.; *J. Mol. Catal. A* **1996**, *114*, 191.
7. Mylonas, A.; Papaconstantinou, E.; *J. Photochem. Photobiol.* **1996**, *94,* 77.
8. Hu, C.; Yue, B.; Yamase, T.; *Appl. Catal., A* **2000**, *194–195*, 99.
9. Ozer, R. R.; Ferry, J. L.; *J. Phys. Chem.* **2000**, *104*, 9444.
10. Anandan, S.; Ryu, S.; Cho, W.; Yoon, M.; *J. Mol. Catal A: Chem.* **2003**, *195*, 201.
11. Ozer, R. R.; Ferry, J. L.; *J. Phys, Chem. B* **2002**, *106*, 4336.
12. Hu, C.; Zhang, Y.; Xu, L.; Peng, G.; *Appl. Catal., A* **1999**, *177*, 237.
13. Stöcker, M.; *Microporous Mesoporous Mater.* **2005**, *82,* 257.
14. Meier, W. M.; Olson, D. H.; *Atlas of Zeolite Structure Types,* 3th ed., Butterworth-Heinemann: Stoneham, 1992.
15. Chen, H.; Matsumoto, A.; Nishimiya, N.; Tsutsumi, K.; *Colloids Surf. A* **1999**, *157*, 295.
16. Kim, Y.; Yoon, M.; *J. Mol. Catal. A: Chem.* **2001**, *168*, 257.

17. Sulikwski, B.; Rachwalik, R.; *Appl. Catal., A* **2003**, *256*, 173.
18. Chen, L. C.; Tsai, F. R.; Huang, C. M.; *J. Photochem. Photobiol. A* **2005**, *170*, 7.
19. Baiocchi, C.; Brussino, M. C.; Pramauro, E.; Prevot, A. B.; Palmisano, L.; Marci, G.; *Int. J. Mass Spectrom*. **2002**, *214*, 247.
20. Guettai, N.; Ait Amar, H.; *Desalination* **2005**, *185*, 439.
21. Nam, W.; Kim, J.; Han, G.; *Chemosphere* **2002**, *47*, 1019.
22. Al-Qaradawi, S.; Salman, S. R.; *J. Photochem. Photobiol. A* **2002**, *148*, 161.
23. P. Chu; *US Pat. 3,709,979* **1972**.
24. Pierella, L. B.; Saux, C.; Bertorello, H. R.; Bercoff, P. G.; Botta, P. M.; Rivas, J.; *Mater. Res. Bull.* **2008**, *43*, 2026.
25. Ito, T.; Inumaru, K.; Misono, M.; *J. Phys. Chem. B* **1997**, *101*, 9958.
26. Pizzio, L. R.; Blanco, M. N.; *Appl. Catal., A* **2003**, *255*, 265.
27. Sulikowski, B.; Haber, J.; Kubacka, A.; Pamin, K.; Olejniczak, Z.; Ptaszyfiski, J.; *Catal. Lett.* **1996**, *39*, 27.
28. Morales-Pacheco, P.; Domínguez, J. M.; Bucio, L.; Alvarez, F.; Sedran, U.; Falco, M.; *Catal. Today* **2011**, *166*, 25.
29. Massart, R.; Contant, R.; Fruchart, J.; Ciabrini, J.; Fournier, M.; *Inorg. Chem.* **1977**, *16*, 2916.
30. Leal Marchena, C.; Frenzel, R. A., Gomez, S.; Pierella, L. B.; Pizzio, L. R.; *Appl. Catal., B* **2013**, *130–131*, 187.
31. Gorsd, M.; Blanco, M.; Pizzio, L. R.; *Appl. Catal., A* **2011**, *400*, 91.
32. Pope, M. T.; *Heteropoly and Isopoly Oxometalates*, Springer-Verlag: Heidelberg, 1983.
33. Rocchiccioli-Deltcheff, C.; Thouvenot, R.; Franck, R.; *Spectrochim. Acta* **1976**, *32 A*, 587.
34. Contant, R.; *Can. J. Chem.* **1987**, *65*, 568.
35. Othman, I.; Mohamed, R. M.; Ibrahim, I. A.; *Appl. Catal., A* **2006**, *299*, 95.
36. Mioc, J. B.; Dimitrijevi, R. Z.; Davidovic, M.; Nedic, Z. P.; Mitrovic, M. M.; Colomban, P.H.; *J. Mater. Sci.,* **1994**, *29*, 3705.
37. Lefebvre, F.; *J. Chem. Soc.* **1992**, 756.
38. Pizzio, L.; Vázquez, P.; Kikot, A.; Basaldella, E.; Cáceres, C.; Blanco, M.; *Stud. Surf. Sci. Catal.* **2002**, *143*, 739.
39. Hasik, M.; Turek, W.; Stochmal, E.; Lapkowski, M.; Pron, A.; *J. Catal.* **1994**, *147*, 511.
40. Su, F.; Zhao, X. S.; Lv, L.; Zhou, Z.; *Carbon* **2004**, *42*, 2821.
41. Decolatti, H. P.; Martínez-Hernández, A.; L. Gutiérrez, B.; Fuentes, G. A.; Zamaro, J. M.; *Microporous Mesoporous Mater.* **2011**, *145*, 41.
42. Pizzio, L. R.; Cáceres, C. V.; Blanco, M. N.; *Appl. Catal., A* **1998**, *167*, 283.
43. Vázquez, P.; Pizzio, L.; Cáceres, C.; Blanco, M.; Thomas, H.; Alesso, E.; Finkielsztein, L.; Lantano, B.; Moltrasio, G.; Aguirre, J.; *J. Mol. Catal. A: Chem.* **2000**, *161*, 223.
44. Zanjanchi, M. A.; Razavi, A.; *Spectrochim. Acta* **2001**, *57*, 119.
45. Fox, M. A.; Cardona, R.; Gaillard, E.; *J. Am. Chem. Soc.* **1987**, *109*, 6347.
46. Tandom, S. P.; Gupta, J. P.; *Phys. Status Solidi* **1970**, *38*, 363.
47. Joselevich, E.; Willner, I.; *J. Phys. Chem.* **1994**, *98*, 7628.
48. Yan, G.; Long, J.; Wang, X.; Li, Z.; Fu, X.; *C. R. Chim.* **2008**, *11*, 114.
49. Coutinho, C. A.; Gupta, V. K.; *J. Colloid Interface Sci.* **2009**, *333*, 457.
50. Iida, Y.; Kozuka, T.; Tuziuti, T.; Yasui, K.; *Ultrasonics* **2004**, *42*, 635.
51. Prevot, A. B.; Fabbri, D.; Pramauro, E.; Baiocchi, C.; Medana, C.; *J. Chromatogr. A* **2008**, *1202*, 145.
52. Spadaro, J. T.; Isabelle, L.; Renganathan, V.; *Environ. Sci. Technol.* **1994**, *28*, 1389.
53. Antonaraki, S.; Triantis, T. M.; Papaconstantinou, E.; Hiskia, A.; *Catal. Today* **2010**, *151*, 119.
54. Mizrahi, D. M.; Saphier, S.; Columbus, I.; *J. Hazard. Mater.* **2010**, *179*, 495.
55. Zhu, C. M.; Wang, L. Y.; Kong, L. R.; Yang, X.; Wang, L. S.; Zheng, S. J.; *Chemosphere* **2000**, *41*, 303.
56. Shankar, M. V.; Cheralathan, K. K.; Arabindoo, B.; Palanichamy, M.; Murugesan, V.; *J. Mol. Catal. A: Chem.* **2004**, *223*, 195.
57. Mahalakshmi, M.; Vishnu Priya, S.; Arabindoo, B.; Palanichamy, M.; Murugesan, V.; *J. Hazard. Mater.* **2009**, *161*, 336.
58. Subba Rao, K. V.; Subrahmanyam, M.; Boule, P.; *Appl. Catal., B* **2004**, *49*, 239.